# Preventing lead leakage in perovskite solar cells with a sustainable titanium dioxide sponge

Salvatore Valastro[1], Emanuele Smecca[1], Giovanni Mannino[1], Corrado Bongiorno[1], Giuseppe Fisicaro[1], Stefan Goedecker[2], Valentina Arena[1], Carlo Spampinato[1,3], Ioannis Deretzis[1], Sandro Dattilo[4], Andrea Scamporrino[4], Sabrina Carroccio[4], Enza Fazio[3], Fortunato Neri[3], Francesco Bisconti[5], Aurora Rizzo[5], Corrado Spinella[1], Antonino La Magna[1] and Alessandra Alberti[1*]

[1] CNR-IMM, Zona Industriale Strada VIII n.5, 95121, Catania, Italy

[2] Department of Physics, University of Basel, Klingelbergstrasse 82, CH-4056 Basel, Switzerland

[3] Dipartimento Scienze Matematiche e Informatiche, Scienze Fisiche e Scienze della Terra, Università Degli Studi di Messina, Viale F. Stagno d'Alcontres 31, 98166 Messina, Italy

[4] CNR-IPCB, Via P. Gaifami 18, 95126, Catania, Italy

[5] CNR NANOTEC – Istituto di Nanotecnologia, c/o Campus Ecotekne, Via Monteroni, 73100 Lecce, Italy

*alessandra.alberti@imm.cnr.it

**Abstract**

**As the market uptake of perovskite solar cells (PSCs) is projected to grow rapidly, this clean energy technology will play an increasingly important role in reducing the global carbon footprint. However, one of the major barriers to its full commercialization is the presence of toxic lead (Pb) which enables the current record in photoconversion efficiency but risks being released into the environment when subjected to water or rain. Here we show that Pb leakage can be prevented by applying a transparent titanium dioxide ($TiO_2$) sponge which allows for an efficient Pb sequestration of 58 ng $cm^{-2}$ $nm^{-1}$. Being already an essential material for PSCs, the additional use of $TiO_2$ through a scalable and solvent-free sputtering process promises extra cost benefits and higher sustainability. Further demonstration of the sponge application with desired thickness on ready-to-use devices, glass, and polymeric foils enforces the practical value of the current approach. Our study provides a sustainable solution to one of the environmental and health risks of PSCs and would accelerate their practical applications.**

Perovskite solar cell (PSC) technologies are acknowledged to represent a tangible breakthrough in the photovoltaic sector due to the high photoconversion efficiency, currently at 25.8% on a lab-scale[1], and low production costs[2,3,4], but some issues continue to impede their commercialization. Although solutions to improve interfaces stability[5] and to rationalize up-scalable production chains[6] have been proposed, the potential release of Pb into the environment remains the most serious concern. It is widely accepted that Pb ions can enter soil and groundwater after being dissolved from residual $PbI_2$ salts by water action on the exposed perovskite film following break events (catastrophic events such as hail, storms, hurricanes or other mechanical failures). $Pb^{2+}$ leaked from perovskite films has been shown in the literature[7] to enter plants, crops, and thus the food cycle ten times more efficiently than Pb contaminants from other Pb-containing electronic devices. This appears to be facilitated by the presence of organic cations such as Methylammonium ($MA^+$) which promotes Pb uptake[8]. Potential Pb leakage can be viewed as a public environmental and health risk source, particularly when PSCs are used in Agrivoltaics[9], Building Integrated and Building Applied Photovoltaics (BIPV and BAPV)[10]. The achievement and maintenance of semi-transparency (ST) along the production chain are key issues for all these applications. Massive production of ST-PSC without concern for the presence of Pb is, indeed, a cross-cutting pivotal challenge.

To address the issue, two approaches can be taken: 1) substitution of Pb with other elements such as tin[11] ($Sn^{2+}$) and 2) direct action against Pb release through targeted strategies. The first approach currently requires significant effort to address compositional stabilization of the perovskite against

$Sn^{2+}$ tendency to change charge state to $Sn^{4+}$. Furthermore, the efficiency record value in tin halide solar cells (~14%[12,13]) is currently far below that of Pb-based solar cells (25.8%), implying that Pb is a necessary actor to accelerate the lab-to-fab-to-market transition.

On the other hand, Pb leakage is reduced by encapsulating materials[14] that protect devices from mechanical damages or by materials that sequestrate Pb via a chemical adsorption mechanism[15]. Encapsulation alone is insufficient to fully prevent Pb leakage from perovskite modules, particularly during breaks in severe weather conditions, and thus Pb-adsorbing layers are required in addition. The ones proposed in the literature[16,17,18,19] are resins or polymers deposited by spin-coating or doctor-blading methods on the surface of transparent conductive oxides (TCO) or on the charges transporting layer (CTL) of the solar cell, with a drawback in complicating the fabrication flow-chart and potentially limiting the charges transport through the device. A recent approach[20] consists of applying a Pb-adsorbing material named P, P'-di(2-ethylhexyl) methanediphosphonic acid (DMDP) (thickness of 5.7 μm) on ethylene-vinyl acetate (EVA) foils which are standard encapsulating materials used in PV technology. This remedy has successfully captured 99.8% of Pb leakage. DMDP was applied on both the front and back sides of the solar cell, increasing material consumption, costs, and complexity. All the aforementioned Pb-adsorbing materials are made using wet chemical methods (**Fig. 1a**) with solvents whose losses contribute to a significant portion of organic pollution[21,22], with disposal of the associated large waste being a further concern[23].

In the literature, there is widespread agreement that titanium dioxide ($TiO_2$) is a material with high adsorption capability towards metal ions[24,25] specifically on Pb[26], for environmental risk mitigation. $TiO_2$ has been used for many purposes over the years, including contaminated water treatments[27] (but never for PSC), because it is non-toxic, low-cost and insoluble in water. In addition, $TiO_2$ is one of the most used and efficient electrons transporting layers (ETLs) in perovskite solar cell architectures[28]. It is fabricated by different techniques like chemical approaches[29] as well as with solvent-free methods like atomic layer deposition[30] and sputtering[31]. Combining the two unique properties of the material would imply that, as soon as a $TiO_2$ layer is enabled for the capture of Pb eventually released from perovskite solar cells, it will pique a huge interest in being integrated into device architecture without high extra costs for equipment investment, well-fitting its rapid industrialization in production flow-charts.

We propose a technological solution to capture Pb from solar devices to support PSC commercialization from a sustainability standpoint. It is based on the use of solvent-free porous $TiO_2$ films that are integrated by physical deposition on ready-to-use devices as the last step of production. The method of integration is applicable to any device architecture and any type of Pb-containing device. The mainstays of the ubiquitous use of the $TiO_2$ sponge are the transparency of the layer and

the deposition process that is done at room temperature. It is demonstrated that the sponge is able to capture Pb leaked from broken PSCs by simulated catastrophic events, and this prevents Pb release into the environment. The $TiO_2$ sponge can sequester Pb in concentrations ranging from 24 g/cm$^{-2}$ to 63 g/cm$^{-2}$, which are equivalently contained in $MAPbI_3$ layers with thicknesses of 200 nm (semi-transparent PSC) and 500 nm (opaque PSC). As a further applicative impact, the $TiO_2$ sponge can be applied to capture Pb from end-of-life perovskite solar cell devices during recycling processes via Pb sequestration and release dedicated cycles.

## Results

### Pb capture from ready-to-use PSCs

$TiO_2$ spongy layers were grown with branched porosity at room temperature (RT) with a Direct Current-pulsed reactive sputtering equipment with a Ti source at grazing incidence and the oxidation occurring in the proximity of the substrate (gig-lox method[32]). The deposition method provides significant benefits such as up-scalability for industrialization and material reproducibility over large areas[33] for increased production throughput. Material waste is inherently avoided (**Fig. 1b**). Deposition at RT enables the integration of $TiO_2$ sponges as the last production step on any kind of ready-to-use PSC architecture. In principle, any other sputtering- or vacuum-based method with recipes that generate porous $TiO_2$ layers at room temperature with extended reactive surfaces can be applied. Despite being already used in the device architecture, $TiO_2$ has never been exploited for leaked Pb sequestration in PSCs, to the best of our knowledge.

As a technological proof-of-concept, we integrated a 340 nm-thick $TiO_2$ layer at RT on a p-i-n PSC made by a stack of ITO/PTAA/$MAPbI_3$-HEC/PCBM/BCP/Au in which the active layer is a 220 nm-thick blend (**Fig. 1c**). The blend, made by $MAPbI_3$ and a small amount of Hydroxyethyl cellulose (HEC), was applied in a recent work[34] to improve the transparency of the perovskite active layer, still maintaining good efficiency for application in BIPV, BAPV and Agrivoltaics.

The $TiO_2$ has been deposited on the back side of the unprotected ready-to-use solar cells, in contact with the Au contacts and the BCP layers. No surface damage or modifications are found after deposition (**Figs.1d-e)**. A first champion outcome is the current density-voltage (J-V) curves collected on the same device before and after deposition. The two curves are identical as shown in **Fig. 1f, Supplementary Fig. 1** and **Table 1**. This demonstrates that no damage/changes occur in all the underlying layers during the sputtering process. It has been also found that the presence of the $TiO_2$ coverage does not cause degradation of the photovoltaic behaviour in the medium-term (60 days) (**Supplementary Fig. 2**). In addition, the Average Transmittance (AVT) value on the PSC covered

with $TiO_2$ and measured in the visible range (400-800 nm) is unmodified at a value of 31.4% (**Supplementary Fig.3**). This is an ideal value for application in BIPV[35] and Agrivoltaics[9].

To investigate the effectiveness of the Pb capture by $TiO_2$, we soaked the devices covered by the oxide layer in 10 mL of deionised water (pH=5.8) for 10 days to permit water to fully infiltrate and dissolve the perovskite layer. Identical devices without $TiO_2$ coverage were soaked in the same amount of water for comparison. Our intent was to simulate extreme rainfall conditions that are nowadays not unusual due to the ongoing severe climate change, and accordingly, we assumed a rainfall rate (rain shower) of 3 cm $h^{-1}$ lasting for 3 hours. In addition, we assumed that the PV maintenance team repaired the damaged panels 10 days after the incident. In the literature works[16,17,18,20], encapsulant materials/glass are used to further cap the devices that are then artificially damaged by a blade cutter or hammer to allow water infiltration through the PSC creeks. In our experiment the PSCs are soaked into $H_2O$ without any type of other encapsulant material, i.e. fully exposed to direct water action. To further worsen the conditions, the vials containing devices in water are mechanically shaken on a flat orbital shaker at a frequency of 200 rpm all over time.

When dipped in water, both uncovered and $TiO_2$-covered devices immediately change colour from brown to yellow (**Supplementary Fig. 4**) reflecting the transformation from $MAPbI_3$ to $PbI_2$. With time, they become more and more transparent marking the complete dissolution of $PbI_2$. This evidence indicates that the $TiO_2$ layer does not act as an encapsulant because it does not prevent water access through the device layers, as expected owing to its characteristic porosity. We used inductively coupled plasma mass spectrometry (ICP/MS) to determine the Pb concentrations in water at the end of the full PSC soaking (**Fig. 1g, left panel**). The concentration of Pb in the water containing the uncovered PSC is 2.65 ppm, a value close to the calculated amount of Pb in 1 $cm^2$ water-exposed area of a 220 nm-thick $MAPbI_3$ (2.90 ppm). Conversely, the Pb concentration in the water containing the $TiO_2$-covered PSC is significantly reduced to 0.26 ppm (average value calculated on three different soaked samples reported in **Supplementary Table 1**), indeed corresponding to a considerable Pb Sequestration Efficiency (SQE) of 90.2%. The data demonstrate that the 340 nm-thick $TiO_2$ layer acts as an efficient filter to capture Pb to minimise its release in water from unprotected (without protective glass coverage) or damaged (with the protective glass broken, as it is shown hereinafter) PSCs. This result was complemented by a similar experiment in which the $TiO_2$ coverage on the PSC was augmented to 1100 nm (**Supplementary Fig. 5).** The density (g $cm^{-3}$) of the upper portion of the $TiO_2$ layer (~20 nm from the surface) measured by X-ray Reflectivity unveils that Pb does not reach the surface in this last case. The finding, joined with the evidence that Pb species are negligibly found in water, leads us to argue that the Pb sequestration within the $TiO_2$ sponge is a bottom-up process that starts at the interface with the device and proceeds upwards likely

assisted by capillary forces.

In the literature papers specifically on leaked Pb sequestration in PSCs[16,17,18,20], water dripping onto damaged encapsulated PSC is studied in addition to soaking. In the wake of those literature works, we implemented an experiment based on water dripping onto damaged encapsulated PSC (**Supplementary Fig. 6**) to simulate heavy rainfall conditions similar to real cases. The results in **Fig. 1g (right panel)** corroborate the role of the $TiO_2$ layer in capturing Pb even under dynamic waterflow circumstances, with average SQE=89% (**Supplementary Table 2**).

**Pb capture in aqueous solutions**

To closely investigate the kinetic of Pb adsorption inside the 340 nm-thick $TiO_2$ layers, we have deposited a layer equivalent to the one used on PSC (340 nm) but on 1.25×1.25 $cm^2$ bare glasses (schematic in **Fig. 2a)**. They have been soaked into three different aqueous solutions of lead-iodide ($PbI_2$) with known Pb ions concentrations (0.4, 1 and 2.2 ppm). As shown in **Fig. 2b**, the $TiO_2$ sequesters a percentage of 90-94% of the initial Pb content in water in the first 4 hours of dipping (the perovskite layer integrated into the devices was dissolved in a couple of hours[20]). This percentage well agrees with the Pb-SQE value measured in soaked PSCs. In the three explored cases, the maximum capture of Pb is limited by its concentration in the solution.

A second figure of merit is that the $TiO_2$ sponge does not release the captured Pb in water for a prolonged dipping time up to 96 hours under continuous mechanical shaking. This evidence demonstrates that the captured Pb is well linked to the oxide and suggests a chemical anchoring onto the $TiO_2$ surfaces.

The adsorption capability of the $TiO_2$ layer was further boosted by soaking it in a more concentrated Pb solution (6.4 ppm). In this case, the Pb capture is limited by the number of available binding sites within the 340 nm of thickness, and therefore the adsorption saturates to a final value of 24 $\mu g_{Pb}$ $cm^{-2}$ (normalized to the $TiO_2$ sample area, inset of **Fig. 2c**). We observe that the Pb capture by $TiO_2$ results in modifications of the optical response of the layer, namely the absorption coefficient and the transmittance of the material, as shown in **Supplementary Fig. 7**.

Now, we explore the Pb-adsorption tunability by varying the film thickness. Indeed, we deposited $TiO_2$ on bare glass with thicknesses of 240, 440 and 1100 nm to soak them into 6.4 ppm of Pb in water solution and monitor the Pb adsorption over time (the same experiment with similar results was done using polymeric foils as substrate). The 240 nm, 440 nm and 1100 nm-thick layers achieve a maximum Pb adsorption of 16 $\mu g_{Pb}$ $cm^{-2}$, 29 $\mu g_{Pb}$ $cm^{-2}$ and 63 $\mu g_{Pb}$ $cm^{-2}$, respectively. These results describe how the $TiO_2$ layer thickness can be engineered according to the specific need, which is

firstly dictated by the perovskite thickness and secondly by the specific architecture and application. Fig. 2c also offers a landscape over the scale-up of the $TiO_2$ thickness that can be fine-tuned on the basis of the specific $MAPbI_3$ thickness integrated into the device: $TiO_2$ sponges in the range of 240-440 nm are able to entirely capture the Pb amount contained in $MAPbI_3$ layers in the range of thickness 70-240 nm, usually applied/needed in ST-PSCs for BIPV and Agrivoltaics[10]; $TiO_2$ layers with thicknesses of 1100 nm allows sequestering all Pb contained into 500 nm-thick $MAPbI_3$ layers used for opaque PSCs. Intermediate conditions can be interpolated. The Pb-adsorption capability (extracted from the linear fit in Fig. 2c) in the $TiO_2$ sponges is ~58 ng $cm^{-2}$ $nm^{-1}$ that is close to what was previously achieved in the literature with chemical DMDP (54 ng $cm^{-2}$ $nm^{-1}$)[16,20]. It has been additionally explored Pb adsorption by the oxide (440 nm-thick) at low pH value to simulate acid rainfall, resulting in 26.1 μg $cm^{-2}$ vs. 27.2 μg $cm^{-2}$ sequestered amount of Pb after 1 day soaking in water at pH 4.5 vs 5.8 (reference), respectively (**Supplementary Fig. 8**)

Similar values of Pb sequestration are obtained for $TiO_2$ deposited on flexible substrates (**Supplementary Fig. 9**) that are indeed enabled for alternative technological schemes. Thus, $TiO_2$ sponges can be deposited on any kind of substrate for direct (on ready-to-use device) or indirect (on glass or foils) capture of Pb, as summarized in **Fig.3**.

**Mechanism of Pb capture**

The $TiO_2$ sponge morphology is schematized in the rendering of **Fig. 4a**. The layer is composed of columnar mesopores (inlet pipelines for host species), 10-50 nm in diameter (**Fig. 4b**), extending through the entire layer thickness and interconnected by a network of branched nanopores with diameters in the range of 1-5 nm[32]. The high magnification scanning transmission electron microscopy (STEM) images in **Figs. 4c-d**, taken after Pb soaking, show, together with oxide branched structure, that Pb (bright regions) is located on the inner wall surfaces of the oxide nano- and mesopores, decorating the exposed areas of the branches. Pb decoration of surfaces is visible through the whole oxide thickness. We further zoomed into the material structure, as shown in the high-resolution image of **Fig. 4e**, to disclose that Pb is uniformly and atomically distributed on the pore surfaces. The presence of Pb was further validated by local spectra acquired by energy dispersive x-ray (EDX) spectroscopy (**Fig. 4f**). Based on all those combined findings, we conclude that the extended surfaces of the $TiO_2$ layer are (all) available and accessible for effective capture of Pb and that Pb is blocked within an oxide-rich environment.

We investigated the adsorption mechanism of a single Pb atom at the inner surfaces of the $TiO_2$ layer with Density Functional Theory (DFT) calculations. Experimental findings[32] suggest that the $TiO_2$

mainly exposes (101) anatase surfaces, whose degree of order depends on whether they are annealed or not. Therefore, the local stoichiometry at the interior terminations forming the three-dimensional cavities can differ from the perfect 1:2 Ti:O ratio. Local oxygen or titanium deficiencies can expose vacancy sites where Pb can be adsorbed.

We model the Pb adsorption taking place at the anatase $TiO_2$ (101) surface (the most stable among low index surfaces[36], named $A_{101}$), considering both the perfect and nonstoichiometric terminations **(Fig. 5a-f, Supplementary Fig. 10 and Supplementary Note 1-3**).

The calculations demonstrate the strong tendency of the Pb impurities to segregate at the $TiO_2$ surfaces where stable oxide-coordinated configurations are gained for permanent loading during and after the immersion in water. X-ray Photoelectron Spectroscopy provided the experimental evidence on the chemisorption of Pb on the $TiO_2$ surfaces based on its coordination with oxygen as shown in **Supplementary Figs. 11-12.**

Theory and experiments converge to explain the reasons for the stable sequestration of Pb and support the cruciality of the pore accessibility and surface reactivity.

## Discussion

To fully support PSC commercialization from a sustainability standpoint, concerns about the presence of Pb need to be rationalised. Such concerns cover a wide range of topics, from manufacturing to field use. Solvents are often applied along the production chain, but their use must be limited to reduce waste. The decision to minimize environmental impact implies that any additional manufacturing step be solvent-free or solvent-poor. Physical deposition methods meet this requirement and are likewise largely exploited by technology manufacturing companies. By applying clean methods, companies additionally meet the requirement to keep costs down thanks to the high manufacturing throughput that pushes commercialization at low-cost. Another concern is about the field use of PSCs. Pb leakage from damaged PSCs is a recurrent theme. It is evident that mitigating the risk of Pb leakage in the event of PSC damage during use necessitates technical solutions that are both affordable and environmentally sustainable. One major risk is in outdoor installations under adverse weather conditions.

The technical solution proposed in the paper is both solvent-free and technologically applicable to large-scale production. It addresses the safe commercialization of any type of Pb-based Perovskite device (e.g., PSC, but also LED, etc.) regardless of the device architecture.

The proposed technical solution entails covering the Perovskite devices with a thin $TiO_2$ sponge using room-temperature sputtering processes. We show that Pb leakage from PSCs can be avoided by this coverage to sequester the metal. Compared to alternative chemically deposited materials, the $TiO_2$

sponge is grown without solvents via sputtering, a clean and up-scalable methodology well suited to high throughput implementation in a manufacturing chain. Sustainability stems from low energy consumption for the production process (large scale production at room temperature) and from the use of vacuum processes. The common use of mesoporous $TiO_2$ layers as ETL in PSC architectures also improves cost assessment since additional equipment investments are not strictly required to apply the same material for Pb sequestration.

We highlighted the multi-branched nature of the $TiO_2$ pores in the sputtered sponge, as well as their full accessibility and high surface reactivity, to ensure effective and long-lasting Pb sequestration. We varied the thickness of the capturing layer in the range 340-1100 nm based on the unique properties of the $TiO_2$ sponge, and this allowed sequestering Pb in a concentration from 24 $g/cm^{-2}$ to 63 $g/cm^{-2}$. Those amounts of Pb are equivalently contained in $MAPbI_3$ layers with thicknesses of 200 nm (semi-transparent PSC) and 500 nm (opaque PSC), respectively.

The observed permanent and stable loading of Pb into the sponge is explained by the favourable interaction of the Pb species with the $TiO_2$ surfaces; it is further supported by DFT calculations. Experimental and theoretical findings provided an atomistic description of the capture mechanism thus enabling the material (unused so far) for application and the sputtering method (likewise any other vacuum-based method that generates porous $TiO_2$ with multi-branched surfaces) for being more intensively scouted. In the near future, the use of sputtered $SnO_2$, another material applied as ETL[37], could be also explored for the same purpose (**Supplementary Note 4-6**, **Supplementary Fig. 13** and **Supplementary Table 5-6**).

Pb sequestration was studied on bare $TiO_2$/glass samples soaked into Pb aqueous solutions and on $TiO_2$ layer deposited on broken PSCs and exposed to continuous dripping of water. In this second case, we integrated the $TiO_2$ sponge as the last production step and at RT on ready-to-use devices. The experiments demonstrate that $TiO_2$ integration by sputtering is easy and has no effect on the photovoltaic performances. Moreover, it has been proved the integration of the $TiO_2$ sponge on extra-coverages (e.g. glass and polymeric foils for further protection), wherein Pb chemisorption and reliable/stable Pb capture are achieved. The use of different substrates thus enables the $TiO_2$ sponge over any technological scheme.

We additionally provided a proof-of-concept experiment on Pb recovery after capture from the $TiO_2$ sponges (**Supplementary Fig. 14**), allowing the material to be reused. Material reuse contributes to the reduction of waste and energy required for complex disposal processes, which is an important step towards sustainability.

Our method represents a concrete proposal for BIPV, BAPV, Agrivoltaics, and opaque devices to prevent Pb release in the environment. It also paves the way for Pb recycling in end-of-life devices.

## Methods

### Chemicals for PSC fabrication

Lead-iodide ($PbI_2$, ultradry 99.999% metals basis) and methylammonium iodide ($CH_3NH_3I$, MAI) were purchased from Alfa Aesar (Kandel, Germany) and GreatCell Solar, respectively. 2-hydroxyethyl cellulose (HEC), dimethyl sulfoxide anhydrous, 99.9% (DMSO); toluene anhydrous, 99.8% (TOL); chlorobenzene anhydrous, 99.8% (CB); 2-propanol (IPA); PTAA [poly(bis{4-phenyl}{2,4,6- trimethylphenyl}amine)]; bathocuproine, 96% (BCP) were purchased from Sigma Aldrich; [6,6]-phenyl $C_{61}$ butyric acid methyl ester (PCBM) was purchased from Nano-c.

### PSC fabrication and characterization

Perovskite solar cells based on a p-i-n architecture were realized employing 15×15×1.1 mm ITO (Indium Tin Oxide) patterned glass as substrates and anode, PTAA as hole transporter layer (HTL), $MAPbI_3$-HEC as a photoactive layer, PCBM as electron transporter material and BCP as hole blocking layer. ITO-glass substrates were cleaned prior to use by ultrasonication baths with deionized water, acetone, 2-propanol, 10 min. at room temperature for each step, and then dried by $N_2$ flow. PTAA (1.5 mg $mL^{-1}$ in Toluene), PCBM (25 mg $mL^{-1}$ in Chlorobenzene) and BCP (0.5 mg $mL^{-1}$ in 2-propanol) were deposited by spin coating, respectively, with the following parameters: 6000 rpm for 30 sec (100 °C for 10 min of annealing), 1000 rpm for 60 sec (no annealing required), 6000 rpm for 20 sec (no annealing required). $MAPbI_3$-HEC solution was obtained by solubilizing 0.76 M of $PbI_2$ and 0.76 M of MAI in DMSO, stirring for 30 min at 80 °C. Next, this solution was added to the HEC powder (11.8 mg of polymer for each mL of $MAPbI_3$) and stirred for 3 h at 80 °C. 45 µl of cooled $MAPbI_3$-HEC was deposited on top of PTAA by spin coating at 12000 rpm for 30 sec and washing with 200 µl of Toluene as antisolvent at the 30$^{th}$ sec, following 30 min of annealing at 100 °C. All materials were deposited in $N_2$ filled glove box (< 0.1 ppm [$O_2$], < 0.1 ppm [$H_2O$]). The device stack was completed by the high vacuum ($8x10^{-7}$ mbar) thermal evaporation (Lesker Co. instrument) of 10 nm of Au as anode top electrode with a deposition rate of 0.4 A $s^{-1}$ and employing a mask that defined a 0.04 $cm^2$ active area. J-V characteristics were measured in ambient air by a digital source meter (Keithley model 2401) under AM 1.5-simulated sunlight (100 mW $cm^{-2}$) from Peccell (PEC-L01) calibrated with a reference Si cell (Peccell PEC-SI01). The scan range was from −0.1 to 1.2 V for the forward scan and from 1.2 to −0.1 V for the reverse scan with a step of 0.01 V. The delay time was of 0.1 s. The scan rate was 50 mV $s^{-1}$.

**$TiO_2$ fabrication**

$TiO_2$ layers were deposited on different substrates (glass, silicon, PEN, PSCs) by a grazing incidence geometry using a customized Magnetron DC-pulsed Sputtering equipment fabricated by Kenosistec s.r.l. The grazing incidence of the titanium source, combined with the local oxidation of the sputtered titanium species near the substrate (gig-lox method) allows for the formation of a spongy fine-branched structure with interconnected mesopores (pipelines) and nanopores that ensure an in-depth pathway of hosts into the porous structure. $TiO_2$ sponges grown at RT offer high surface exposure[32] and reactivity. As a matter of fact, we previously applied them for gas sensing (active layer)[33,38], molecular functionalization[39] and photovoltaics (ETL for PSC)[40], taking additional advantages from the material transparency. To grow the $TiO_2$ layers for Pb capture, the flowrate of the carrier gas (Ar) and the reactive gas ($O_2$) is set to 69 and 2 sccm, respectively. A pre-sputtering step of 1 min is performed before the deposition process to clean up the surface of the Titanium target to remove oxidised layers. The deposition is done at room temperature using a power of 140 W, a current of 424 mA and a voltage of 330 V (power loading 6.9 W $cm^{-2}$). The deposition rate is equal to 3.4 nm $min^{-1}$. The thickness of $TiO_2$ is regulated by varying the deposition time. Deposition can be done up to 4 inches wafers in our equipment, as shown in a previous paper dedicated to the use of $TiO_2$ for environmental gas detection[33] (US patent)[41], with further scale-up feasible in dedicated industrial equipment.

**Absorption and transmittance measurements**

Absorption coefficient and transmittance measurements are collected by using a V-VASE, J.A. Woollam spectroscopic ellipsometer equipped with a monochromator and autoretarder. The AVT is calculated from the arithmetic mean of the 400–800 nm transmittance range.

**Pb-adsorption characterization**

Different amounts of $PbI_2$ (Sigma-Aldrich, 99.99% purity) were dissolved in 10 mL of deionized water (pH=5.8) to tune the Pb concentration. 1.25×1.25 $cm^2$ $TiO_2$ samples with different thicknesses were soaked in Pb aqueous solutions. Samples were mechanically shaken over time at 200 rpm with a flat orbital shaker (IKA KS 260 basic). Pb concentrations were determined with an ICP/MS Nexion 300X using the kinetic energy discrimination mode (KED) for interference suppression. Before analysis, samples were diluted, acidified with nitric acid, and added to the internal standards required to determine. Each determination was performed three times. The accuracy of the analytical determination was confirmed by measuring a standard reference material, SRM 1643f - Trace

Elements in Water, without observing an appreciable difference. The acid solution at pH 4.5 was prepared by withdrawing 20 µL of HCl from a stock solution 0.1 M and diluting them up to 40 mL with distilled water at pH 5.8. pH values were registered by HI2211 pH ORP meter. At least 3 measurements were collected to assess the pHs of both distilled and acid water. The PSC samples were soaked in 10 mL of such solutions (pH 5.8 and 4.5) under shaking for 24h. 100 µL of solution for each sample was picked up and diluted to 5 mL to perform ICP-MS analysis obtaining a standard deviation that does not exceed 2%.

**STEM and EDX analyses**

Preparation was carried out in a standard mechanical way and final ion milling process on the $TiO_2$ sample with the maximum Pb uptake (soaked in 6.4 ppm Pb water solution for 96 hours). STEM analyses were carried out with a Cs-corrected JEOL ARM200C at 200 keV, equipped with 100 $mm^2$ JEOL energy dispersive X-ray (EDX) detector. STEM images were acquired in scanning mode using the HAADF detector. Pb atoms proved to be very stable under electron illumination, despite their atomically dispersed fashion. All the data analysis and elemental quantification were carried out with Gatan Microscopy suite v3.4.

**Density Functional Theory Calculations**

The Kohn-Sham density functional theory (DFT) has been employed within the BigDFT package[42,43], using wavelets as basis functions. Soft norm-conserving pseudo-potentials including non-linear core corrections[44,45] along with the Perdew-Burke-Ernzerhof functional were used to describe the core electrons and exchange-correlation as implemented in the Libxc[46] library. We performed all runs with equivalent parameter settings and convergence criteria. All structures were relaxed using the Hellman-Feynman scheme until forces were less than 5.0 meV $Å^{-1}$. The lattice parameters of the conventional anatase cell were optimized using a 4×4×2 *k*-point Monkhorst-Pack grid until the pressure converged below 0.05 kbar, obtaining a cell with lattice constants a=3.79 Å and b=9.71 Å. The experimental lattice constants are a=3.79 Å and b=9.625 Å [47]. The anatase $TiO_2$ (101) surface was modelled with six layers of a 4×1 supercell (288 atoms in total), starting from the optimized bulk lattice parameters with periodic dimensions of 15.18 Å and 10.43 Å[48]. The first layer is the outermost in contact with vacuum or water. Atoms at the bottom layer were fixed at their bulk coordinates to emulate bulk behaviour. The 4×1 periodicity prevents spurious interactions with periodic images. Surface boundary conditions and a wavelet uniform mesh of $h_{grid} := h_x = h_y = h_z = 0.40$ Bohr have been set for all calculations. Only the Γ point has been used for the *k*-space integration. A water

environment has been included by means of the soft-sphere implicit solvation model[49,50,51]. When solvent effects are considered, one surface is considered to be in contact with the implicit solvent. For the opposite (bottom) surface, vacuum conditions are always used by setting a large radius of the soft-sphere model for bottom atoms. Water has a relative permittivity of 78.36 at T=20 °C[52].The soft-sphere model parameters are reported in Ref.[50].

**XPS analyses**

X-ray Photoelectron Spectroscopy (XPS) spectra were acquired using the K-alpha system of Thermo Scientific, equipped with a monochromatic Al-Ka source (1486.6 eV), operating in a constant analyser energy (CAE) mode with a pass energy of 20 eV for high resolution spectra and a spot size of 400 mm.

**XRR analyses**

X-Ray Reflectivity analyses were done using a D8Discover Bruker AXS diffractometer equipped with a Cu-kα source, a Goebel mirror, and a scintillator for detecting the reflected X-ray beam. The critical angle was measured correspondingly to a penetration depth of ~20 nm in the $TiO_2$ material. This parameter is sensitive to the electronic density of the material within the surface layer.

**Estimation of Pb amount in $MAPbI_3$ layers**

The $MAPbI_3$ density[53] is assumed equal to 4 g $cm^{-3}$. The mass percentage of Pb with respect $MAPbI_3$ is 33.4% (207.2u/620u). Considering an area of 1 $cm^2$ and a film thickness of 220 nm, the volume of $MAPbI_3$ is ~$2.2\times10^{-5}$ $cm^3$, with an amount of 29 μg of Pb. Consequently, in 10 mL of water, the Pb concentration is ~2.9 ppm.

**Calculation of Pb sequestration efficiency (SQE)**

Pb sequestration efficiency (SQE) is calculated with the following formula:

$$SQE = 1 - \frac{Pb\ leakage\ from\ devices\ covered\ with\ gig{-}lox\ TiO_2}{Pb\ leakage\ from\ devices\ uncovered} \quad (1)$$

**Data availability statements**

The data supporting the findings of this study are available within this paper and the Supplementary Information. Source data are provided with this paper.

**Acknowledgements**

This activity was partially supported at CNR by the national projects, BEYOND NANO Upgrade (CUP G66J17000350007) and VertiGrow (CUP B15F21004410005). This work has been partially funded by European Union (NextGeneration EU), through the MUR-PNRR project SAMOTHRACE- SiciliAn MicronanOTecH. Research And Innovation CEnter- (ECS00000022, CUP B63C22000620005). This work was supported by a grant from the Swiss National Supercomputing Centre (CSCS) under project ID s963 and s1167. The authors thank Teresia Quinn for her kind proof-reading work. The authors thank Vittorio Privitera, head of CNR-IMM, for supporting the research.

**Author Contributions Statement**

S.V conceived the idea of the experiment, coordinated data analyses and cross-correlations, wrote the paper; E.S. and V.A performed XRR measurements; C.B. carried out STEM and EDX analyses; S.D, A.S. and S.C. conducted Pb sequestration measurements; F.B. and A.R. fabricated perovskite solar cells; G.M and C.S performed spectroscopic ellipsometry measurements; G.F., I.D. and S.G. carried out DFT calculations; E.F. and F.N. performed XPS analysis; A.L. and C.S. supervised the research. A.A. planned and coordinated the experiments, data analyses, collaborations and fundings. All authors reviewed the paper.

**Competing Interests Statement**

The authors declare no competing interests.

**Tables**

| | before $TiO_2$ deposition (RS) | after $TiO_2$ deposition (RS) |
|---|---|---|
| $V_{OC}$ (V) | 1.06 | 1.06 |
| $J_{SC}$ (mA $cm^{-2}$) | 15.2 | 15.3 |
| FF (%) | 71.7 | 72.0 |
| PCE (%) | 11.6 | 11.7 |

**Table 1** Photovoltaic Parameters (reverse scan) of the PSCs before and after the $TiO_2$ deposition.

## Figures

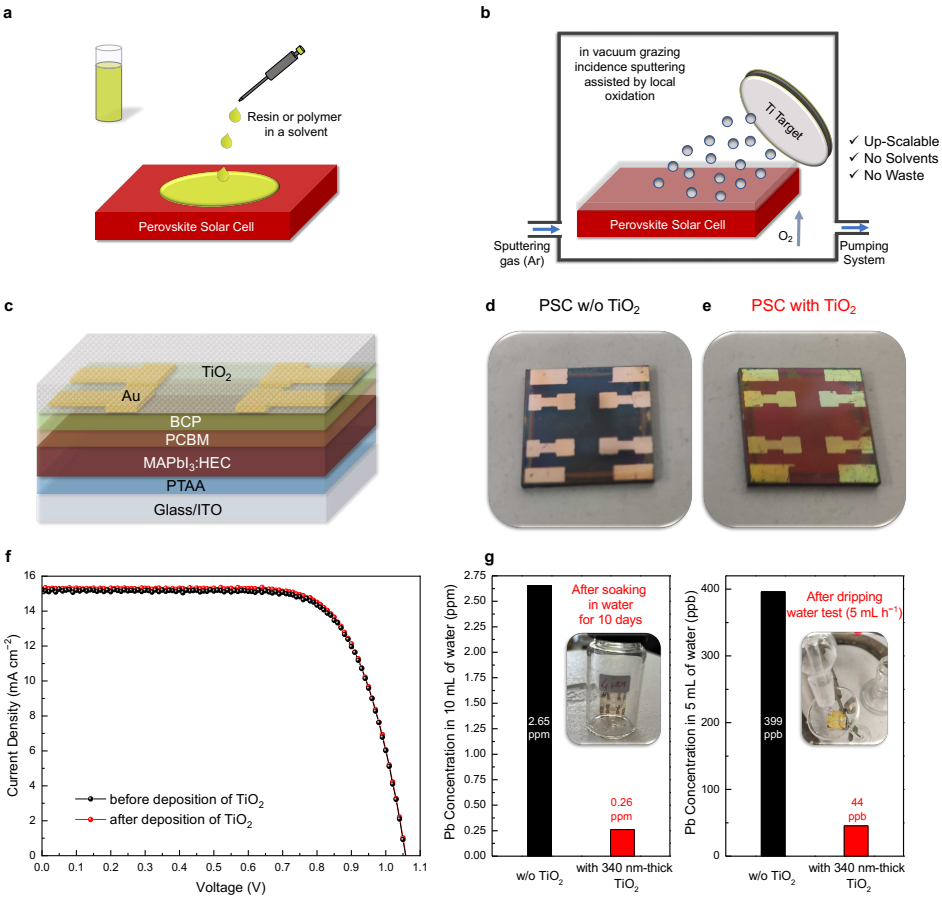


**Fig. 1 Pb capture by $TiO_2$ sponges integrated on PSCs. a** Pb-adsorbing materials fabricated by wet chemical approaches vs **b** $TiO_2$ fabricated by dry physical method. **c** Architecture of a semi-transparent perovskite solar cell with the $TiO_2$ layer directly deposited on it. Photo of the PSC before **d** and after **e** the $TiO_2$ deposition. **f** Representative current density vs. voltage curves (J-V) of the PSCs before and after the $TiO_2$ deposition. **g** Left panel: Pb concentration after 10 days of soaking in 10 mL of water of PSCs with and without $TiO_2$. The values are calculated in average on three soaked PSC devices (error bars in Supplementary Table 1). Right panel: Pb concentration after 1h of water dripping at flow rate of 5 mL $h^{-1}$ over artificially damaged PSC devices with and without the $TiO_2$ layer to simulate a heavy rainfall of 50 mm $h^{-1}$ flowing through the frontside cracks (Supplementary Fig. 6). The values are calculated in average on three PSC devices, each type (Supplementary Table 2). In 1h of dripping, ~8% of the overall pristine Pb amount contained into the perovskite layer is found in the collected water at the exit from the sample without $TiO_2$ (399 ppb in 5mL of water), whilst the sponge is seen to capture ~89% (44 ppb in 5 mL of water) of the leaked Pb, in average, in the devices provided with the $TiO_2$ bottom coverage.

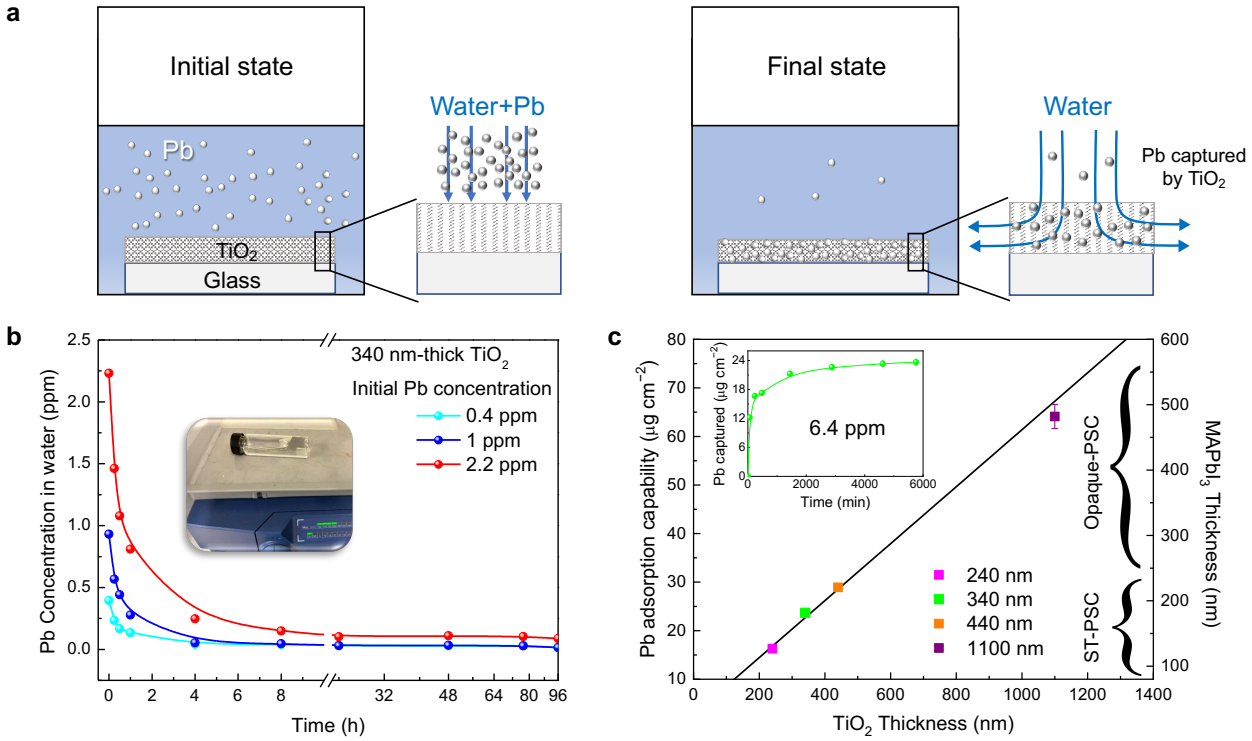


**Fig. 2 Pb capture by $TiO_2$ sponges in aqueous solutions. a** Schematic of the experimental setup: 340 nm-thick $TiO_2$ layers deposited on bare glass soaked into Pb-containing water solution. **b** Pb concentration in water vs time for 340 nm-thick $TiO_2$ layers soaked into different Pb-concentrated water solution: the final Pb-concentration values measured in water are 14.5, 14.8 and 88.1 ppb, for 0.4 ppm, 1 ppm and 2.2 ppm respectively. The inset is the sample into the vial over the mechanical shaker, continuously working at 200 rpm for 96 hours (it was not necessary to prolong to 10 days due to value saturation). The error bars in Pb concentration measurements by ICP/MS is 1%. The experiment also demonstrates that the $TiO_2$ sponge is effective in capturing Pb from its top, according to the peculiar, branched porosity with vertical pipelines across the entire layer thickness. **c** Pb adsorption capability values, with error bars (propagation of uncertainty), measured in 3 samples for each thickness of $TiO_2$ (240, 340, 440 nm) soaked in 6.4 ppm Pb water solution (a representative kinetic curve of the Pb captured into 340nm-thick $TiO_2$ layer is shown in the inset). Data are presented as mean values +/−SD. The calculated Pb-adsorption capability is 70 ng $cm^{-2}$ $nm^{-1}$ in 340nm of $TiO_2$ and ~58 ng $cm^{-2}$ $nm^{-1}$ in the range 240-1100 nm from the linear fit in Fig. 2c. The sequestrated Pb is made in relationship (right axis) with the corresponding $MAPbI_3$ thickness, once all Pb contained in the film is dissolved in water. Thereby, a $TiO_2$ layer in the range of thickness 240-440 nm entirely sequesters the Pb contained in Semi-Transparent (ST) PSCs (70-240 nm). If thicker $TiO_2$ layers are grown (e.g.1100 nm), they can be also used for the full Pb capture in opaque PSCs.

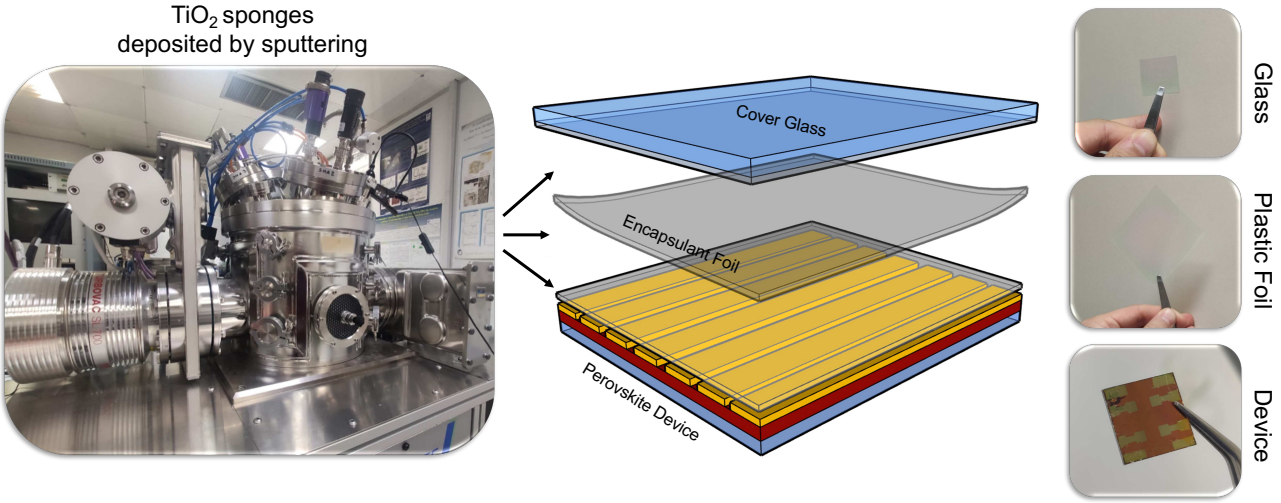


**Fig.3. Possible schemes for the $TiO_2$ sponge integration.** Sputtering equipment used for $TiO_2$ deposition and possible schemes for the layer integration on any kind of substrate for direct (on ready-to-use device) or indirect (on glass or foils) capture of Pb. The Pb adsorption capability in $TiO_2$ sponges does not depend on the substrate used. Supplementary Fig. 9 shows a comparative capturing behaviour in oxide layers deposited on glass and Polyethylene naphthalate (PEN) foils. The arrows indicate the side wherein the oxide can be applied (transparent grey layer in the rendering). Bifacial depositions are also feasible. The pictures on the right panel are taken on proof-of-concept samples immediately after deposition. The $TiO_2$ layer deposition is done at RT for the preservation of materials and devices; it also guarantees high surface reactivity and durable capture. The method is at zero-waste production and at zero-solvent use. Pb sequestration in end-of-life devices can be engineered by $TiO_2$ capturing surfaces, using flat or bent surfaces, for recycling purposes.

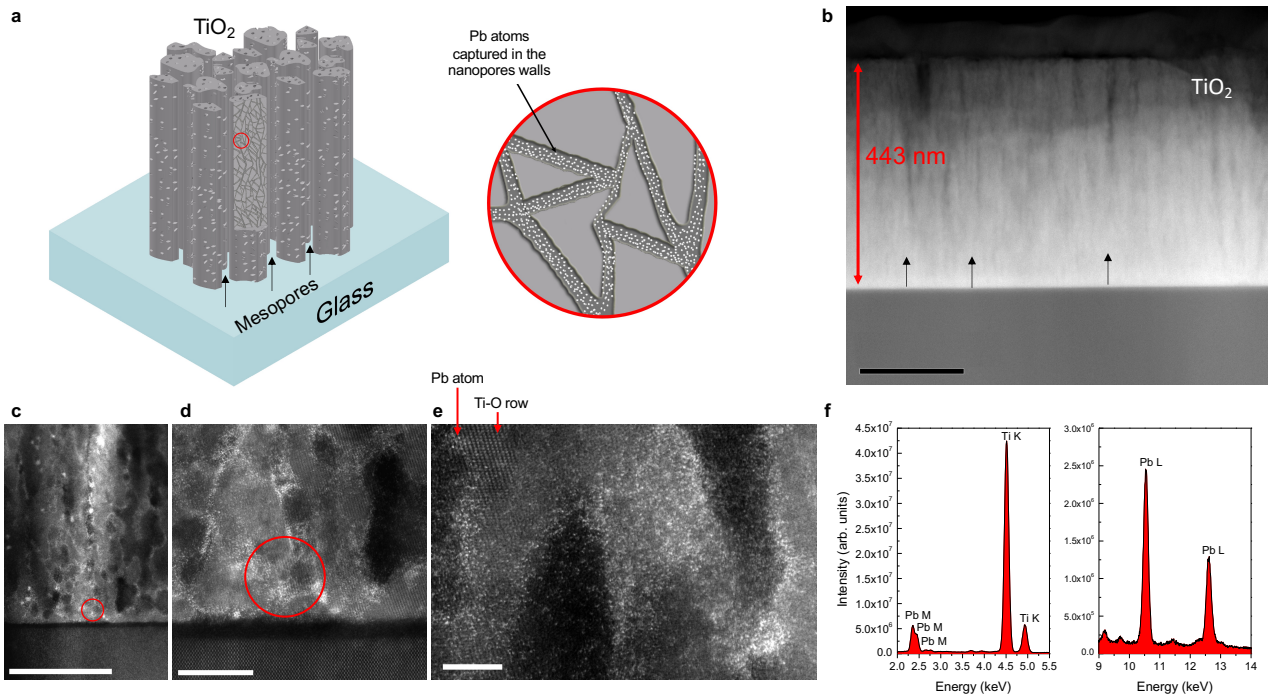


**Fig. 4 Mechanism of Pb capture by $TiO_2$ sponges. a** Rendering of the $TiO_2$ nanostructure wherein we highlight the oxide rod structure, the vertical mesopores (indicated by the black arrows), and the inner branched structure of nanopores also connected to the mesopores that serves as inlet pipelines. **b** Cross-sectional STEM image of a 440 nm-thick $TiO_2$ layer (scale bar=200 nm), wherein the mesopores have a dark contrast (some of them labelled by vertical arrows). Note that the mesopores cross the entire layer from the interface to the surface. **c**-**e** STEM image sequence that zooms into the $TiO_2$ sponge after Pb sequestration. Pb is uniformly captured all over the surfaces of the wall of the $TiO_2$ nano and mesopores. Note in **e** the Ti-O rows within the atomic planes taken in high resolution and the brilliant extra-spots that are, instead, Pb captured species. Pb atoms are clearly identifiable in comparison with the Ti-O ordered rows due to the mass contrast (Pb=207.2u, Ti=47.9u). The scale bars of **c**, **d** and **e** are 50 nm, 10 nm, and 5 nm, respectively. **f** integrated EDX spectrum taken inside the circled area showing L and M shell peaks of Pb along with K shell peaks of Ti.

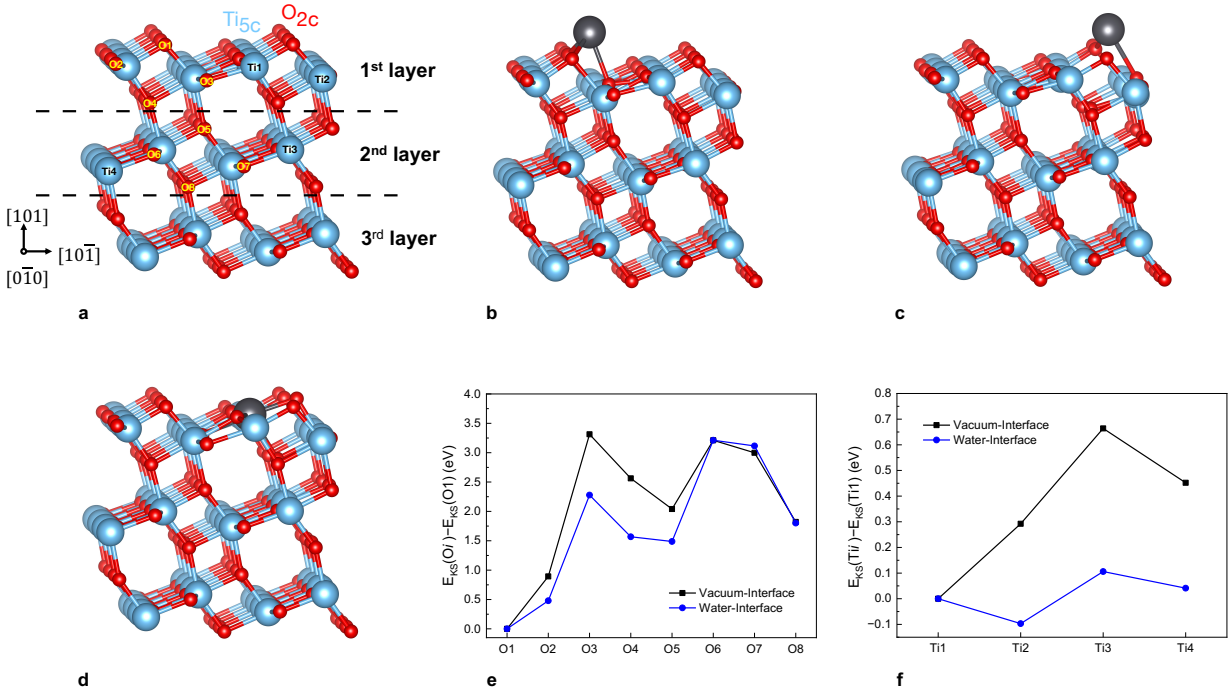


**Fig. 5 First principles DFT simulations of Pb adsorption on $TiO_2$. a** Ball and stick model of the $A_{101}$ 4×1 supercell. *Ab-initio* analysis highlights a strong adsorption interaction of a Pb atom (grey) both at the perfect and nonstoichiometric $A_{101}$ in contact with vacuum or water environment. Stable adsorption configurations are characterized by Pb-O (red) bonds rather than Pb-Ti (cyan) ones in all cases. **b**, in the perfect $A_{101}$, a Pb atom binds to three outermost oxygens forming three O-Pb bonds in the same way at the vacuum and at the water interface. The strong interaction between Pb and $A_{101}$ is quantified by the large adsorption energy (Supplementary Note 1-3 and Supplementary equation (1)) of 3.40 eV at the $A_{101}$/vacuum interface and 2.49 eV at the $A_{101}$/water interface (Supplementary Table 3). The substitution of Pb with an O1-O8 oxygen atom of the first two O-Ti-O layers, hence modelling the Pb adsorption on an $A_{101}$ surface with an oxygen vacancy, is highly unstable and brings strong local atomic adjustments characterized by the tendency to increase the number of Pb-O bonds. Replacing Pb with Ti, hence mimicking Pb adsorption on an $A_{101}$ surface with a deficit of titanium, induces negligible structural rearrangements (Supplementary Fig. 10 and Supplementary Table 4). Among various adsorption sites of the first two O-Ti-O layers at the nonstoichiometric surface, a Pb atom prefers to lie at outermost sites O1 **c** or Ti1 **d**. Only at the $A_{101}$/water interface, Ti2 is slightly energetically more favourable. **e** Change of the Kohn-Sham total energy of all O1-O8 optimized configurations of Supplementary Fig. 10 with respect to the energy of the O1 adsorption case. **f**, energy differences between various Ti1-Ti4 adsorption sites are below 1 eV, with such differences even below 100 meV in the case of the $A_{101}$/water interface.

## References


[1] H. Min et al. Perovskite solar cells with atomically coherent interlayers on $SnO_2$ electrodes. *Nature* **598**, 444–450 (2021)
[2] Jena, A. K., Kulkarni, A. & Miyasaka, T. Halide perovskite photovoltaics: background, status, and future prospects. *Chem. Rev.* **119**, 3036–3103 (2019).
[3] Rong, Y. et al. Challenges for commercializing perovskite solar cells. *Science* **361**, eaat8235 (2018).
[4] Mathews, I. et al. Economically Sustainable Growth of Perovskite Photovoltaics Manufacturing. *Joule* **4**, 822–839 (2020)
[5] Khenkin, M.V. et al. Consensus statement for stability assessment and reporting for perovskite photovoltaics based on ISOS procedures. *Nat. Energy* **5**, 35–49 (2020)
[6] Reddy, S.H., Di Giacomo, F., Di Carlo, A. Low-Temperature-Processed Stable Perovskite Solar Cells and Modules: A Comprehensive Review. *Adv. Energy Mater.* **12**, 2103534 (2022)
[7] Li, J. et al. Biological impact of lead from halide perovskites reveals the risk of introducing a safe threshold. *Nat. Commun.* **11**, 310 (2020).
[8] Ponti, C. et al. Environmental lead exposure from halide perovskites in solar cells. *Trends in Ecology & Evolution* **37**, 281–283 (2022)
[9] Gorjian, S. et al. Progress and Challenges of crop production and electricity generation in agrivoltaic systems using semi-transparent photovoltaic technology. *Renew. Sust. Energ. Rev.* **158,** 112126 (2022)
[10] Koh, T.M. et al. Halide Perovskite Solar Cells for Building Integrated Photovoltaics: Transforming Building Façades into Power Generators. *Adv. Mater.* **34**, 2104661 (2022)
[11] Pitaro, M., Tekelenburg, E.K., Shao, S., Loi, M.A. Tin Halide Perovskites: From Fundamental Properties to Solar Cells. *Adv.Mater.* **34**, 2105844 (2022)
[12] Jiang, X. et al. One-Step Synthesis of $SnI_2$·$(DMSO)_x$ Adducts for High-Performance Tin Perovskite Solar Cells. *J. Am. Chem. Soc.* **143**, 10970–10976 (2021)
[13] Sanchez-Diaz, J. et al. Tin perovskite solar cells with >1,300 h of operational stability in $N_2$ through a synergistic chemical engineering approach. *Joule* **6**, 861–883 (2022)
[14] Jiang, Y. et al. Reduction of lead leakage from damaged lead halide perovskite solar modules using self-healing polymer-based encapsulation. *Nat. Energy* **4**, 585–593 (2019).
[15] Ravi, V.K., Mondal, B., Nawale, VV. & Nag, A. Don't Let the Lead Out: New Material Chemistry Approaches for Sustainable Lead Halide Perovskite Solar Cells. *ACS Omega* **5**, 29631–29641 (2020)
[16] Li, X. et al. On-device lead sequestration for perovskite solar cells. *Nature* **578**, 555–558 (2020).
[17] Chen, S. et al. Trapping lead in perovskite solar modules with abundant and low-cost cation exchange resins. *Nat. Energy* **5**, 1003–1011 (2020).
[18] Chen, S. et al. Preventing lead leakage with built-in resin layers for sustainable perovskite solar cells. *Nat. Sustain.* **4**, 636–643 (2021)
[19] Lee, J., Kim, G.-W., Kim, M., Park, S. A. & Park, T. Nonaromatic Green-Solvent-Processable, Dopant-Free, and Lead-Capturable Hole Transport Polymers in Perovskite Solar Cells with High Efficiency. *Adv. Energy Mater.* **10**, 1902662 (2020)
[20] Li, X., Zhang, F., Wang, J. et al. On-device lead-absorbing tapes for sustainable perovskite solar cells. *Nat. Sustain.* **4**, 1038–1041 (2021)
[21] Clarke, CJ., Tu, W., Levers, O., Bröhl, A. & Hallett, JP. Green and Sustainable Solvents in Chemical Processes. *Chem. Rev.* **118**, 747–800 (2018)
[22] Albini, A., Protti, S. (2016). The Solvent Issue. In: Paradigms in Green Chemistry and Technology. SpringerBriefs in Molecular Science. Springer, Cham.
[23] Chea, JD. Evaluation of Solvent Recovery Options for Economic Feasibility through a Superstructure-Based Optimization Framework. *Ind. Eng. Chem. Res.* **59**, 5931–5944 (2020)
[24] Giammar, DE., Maus, CJ. & Xie, L. Effects of Particle Size and Crystalline Phase on Lead Adsorption to Titanium Dioxide Nanoparticles. *Environ. Eng. Sci.* **24**, 85–95 (2007)
[25] Zhao, X. Jia, Q., Song, N., Zhou, W. & Li, Y. Adsorption of Pb(II) from an Aqueous Solution by Titanium Dioxide/Carbon Nanotube Nanocomposites: Kinetics, Thermodynamics, and Isotherms. *J. Chem. Eng. Data* **55**, 4428–4433 (2010)
[26] Liang, P., Qin, Y. C., Hu, B., Peng, T. Y. & Jiang, ZC. Nanometer-size titanium dioxide microcolumn on-line preconcentration of trace metals and their determination by inductively coupled plasma atomic emission spectrometry in water. *Anal. Chim. Acta* **440**, 207–213 (2001)
[27] Lee, S., Park, S. $TiO_2$ photocatalyst for water treatment applications. *J. Ind. Eng. Chem.* **19**, 1761–1769, 2013
[28] Jacobsson, TJ. et al. An open-access database and analysis tool for perovskite solar cells based on the FAIR data principles. *Nat. Energy* **7**, 107–115 (2022)
[29] Kim, M. et al. Conformal quantum dot–$SnO_2$ layers as electron transporters for efficient perovskite solar cells. *Science* **375**, 302–306 (2022).
[30] Seo, S. et al. Amorphous $TiO_2$ Coatings Stabilize Perovskite Solar Cells. *ACS Energy Lett.* **6**, 3332–3341 (2021)
[31] Alberti, A. et al. Nanostructured $TiO_2$ Grown by Low-Temperature Reactive Sputtering for Planar Perovskite Solar Cells. *ACS Appl. Energy Mater.* **2**, 6218–6229 (2019)

[32] Sanzaro, S. et al. Multi-Scale-Porosity $TiO_2$ scaffolds grown by innovative sputtering methods for high throughput hybrid photovoltaics. *Sci. Rep.* **6,** 39509 (2016)
[33] Alberti, A. et al. Innovative spongy $TiO_2$ layers for gas detection at low working temperature. *Sens. Actuators B: Chem.* **259**, 658–667 (2018)
[34] Bisconti, F. et al. Managing transparency through polymer/perovskite blending: A route toward thermostable and highly efficient, semi-transparent solar cells. *Nano Energy* **89**, 106406 (2021)
[35] Giuliano, G., Bonasera, A., Arrabito, G. & Pignataro, B. Semitransparent Perovskite Solar Cells for Building Integration and Tandem Photovoltaics: Design Strategies and Challenges. *Sol. RRL* **5**, 2100702 (2021)
[36] Diebold, U. The Surface Science of Titanium Dioxide. *Surf. Sci. Rep.* **48**, 53–229 (2003)
[37] Park, S.Y. & Zhu, K. Advances in $SnO_2$ for Efficient and Stable n–i–p Perovskite Solar Cells. *Adv. Mater.* **34**, 2110438 (2022)

## Methods' References

[38] Smecca, E. et al. Porous Gig-Lox $TiO_2$ Doped with $N_2$ at Room Temperature for P-Type Response to Ethanol. *Chemosensors* **7**, 12 (2019)
[39] Sanzaro, S. et al. Pervasive infiltration and multi-branch chemisorption of N-719 molecules into newly designed spongy $TiO_2$ layers deposited by gig-lox sputtering processes. *J. Mater. Chem. A* **5**, 25529–25538 (2017)
[40] Sanzaro, S. et al. Bimodal Porosity and Stability of a $TiO_2$ Gig-Lox Sponge Infiltrated with Methyl-Ammonium Lead Iodide Perovskite. *Nanomaterials* **9**, 1300 (2019)
[41] Alberti, A., Renna, L., Gervasi, L., Smecca, E., Sanzaro, S., Galati, C., Santangelo, A., La Magna, A., MOx-based gas sensor and manufacturing method thereof, US patent n°10871462B2, granted on 2020-12-22
[42] Ratcliff, L. E. et al. Flexibilities of wavelets as a computational basis set for large-scale electronic structure calculations. *J. Chem. Phys.* **152**, 194110 (2020)
[43] BigDFT software package. http://www.bigdft.org, Accessed: 23-02-2022.
[44] Goedecker, S., Teter, M. & Hutter, J. Separable Dual-Space Gaussian Pseudopotentials. *Phys. Rev. B* **54**, 1703–1710 (1996)
[45] Willand, A. et al. Conserving Pseudopotentials with Chemical Accuracy Compared to All-Electron Calculations. *J. Chem. Phys.***138**, 104109 (2013)
[46] Marques, M. A., Oliveira, MJ., Burnus & T. Libxc: A Library of Exchange and Correlation Functionals for Density Functional Theory. *Comput. Phys. Comm.* **183**, 2272–2281 (2012)
[47] Reddy, KM., Manorama, SV. & Reddy, AR. Bandgap Studies on Anatase Titanium Dioxide Nanoparticles. *Mater. Chem. Phys.* **78**, 239–245 (2003)
[48] Fisicaro, G. et al. Wet Environment Effects for Ethanol and Water Adsorption on Anatase TiO2 (101) Surfaces. *J. Phys. Chem. C* **124**, 2406–2419 (2020)
[49] Fisicaro, G., Genovese, L., Andreussi, O., Marzari, N. & Goedecker, S. A Generalized Poisson and Poisson-Boltzmann Solver for Electrostatic Environments. *J. Chem. Phys.* **144**, 014103 (2016)
[50] Fisicaro, G. et al. Soft-Sphere Continuum Solvation in Electronic-Structure Calculations. *J. Chem. Theory Comput.* **13**, 3829–3845 (2017)
[51] Andreussi, O. & Fisicaro, G. Continuum Embeddings in Condensed-Matter Simulations. *Int. J. Quantum Chem.* **119**, e25725 (2019)
[52] Buckley, F. & Maryott, AA. Tables of Dielectric Dispersion Data for Pure Liquids and Dilute Solutions; U.S. Dept. of Commerce, National Bureau of Standards, 6–8 (1958)
[53] Wei, H. & Huang, J. Halide lead perovskites for ionizing radiation detection. *Nat. Commun.* **10**, 1066 (2019).